NOTICE

This report was prepared by Rensselaer Polytechnic Institute as a result of research sponsored by the National Center for Earthquake Engineering Research (NCEER) through grants from the National Science Foundation, the New York State Science and Technology Foundation, and other sponsors. Neither NCEER, associates of NCEER, its sponsors, Rensselaer Polytechnic Institute, nor any person acting on their behalf:

a. makes any warranty, express or implied, with respect to the use of any information, apparatus, method, or process disclosed in this report or that such use may not infringe upon privately owned rights; or

b. assumes any liabilities of whatsoever kind with respect to the use of, or the damage resulting from the use of, any information, apparatus, method or process disclosed in this report.

Any opinions, findings, and conclusions or recommendations expressed in this publication are those of the author(s) and do not necessarily refect the views of NCEER, the National Science Foundation, the New York State Science and Technology Foundation, or other sponsors.

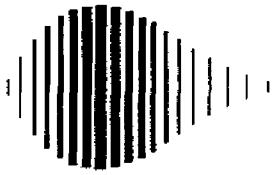

Longitudinal Permanent Ground Deformation Effects on Buried Continuous Pipelines

by

M.J. O'Rourke[1] and C. Nordberg[2]

June 15, 1992

Technical Report NCEER-92-0014

NCEER Project Number 90-3003

NSF Master Contract Number BCS 90-25010
and
NYSSTF Grant Number NEC-91029

1 Professor, Department of Civil Engineering, Rensselaer Polytechnic Institute
2 Graduate Research Assistant, Department of Civil Engineering, Rensselaer Polytechnic Institute

NATIONAL CENTER FOR EARTHQUAKE ENGINEERING RESEARCH
State University of New York at Buffalo
Red Jacket Quadrangle, Buffalo, NY 14261

PREFACE

The National Center for Earthquake Engineering Research (NCEER) was established to expand and disseminate knowledge about earthquakes, improve earthquake-resistant design, and implement seismic hazard mitigation procedures to minimize loss of lives and property. The emphasis is on structures in the eastern and central United States and lifelines throughout the country that are found in zones of low, moderate, and high seismicity.

NCEER's research and implementation plan in years six through ten (1991-1996) comprises four interlocked elements, as shown in the figure below. Element I, Basic Research, is carried out to support projects in the Applied Research area. Element II, Applied Research, is the major focus of work for years six through ten. Element III, Demonstration Projects, have been planned to support Applied Research projects, and will be either case studies or regional studies. Element IV, Implementation, will result from activity in the four Applied Research projects, and from Demonstration Projects.

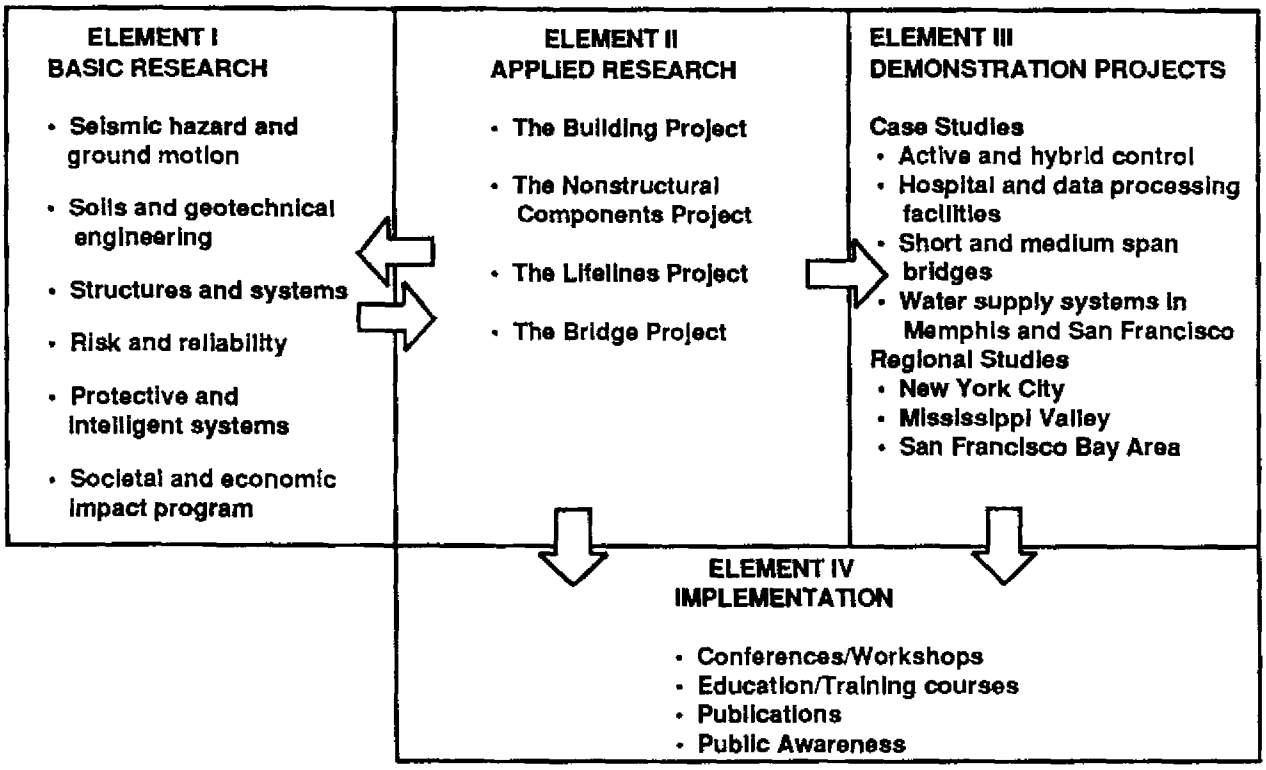

Research tasks in the **Lifeline Project** evaluate seismic performance of lifeline systems, and recommend and implement measures for mitigating the societal risk arising from their failures caused by earthquakes. Water delivery, crude oil transmission, gas pipelines, electric power and telecommunications systems are being studied. Regardless of the specific systems to be considered, research tasks focus on (1) seismic vulnerability and strengthening; (2) repair and restoration; (3) risk and reliability; (4) disaster planning; and (5) dissemination of research products.

The end products of the **Lifeline Project** will include technical reports, computer codes and manuals, design and retrofit guidelines, and recommended procedures for repair and restoration of seismically damaged systems.

The **soils and geotechnical engineering program** constitutes one of the important areas of research in Element I, **Lifelines Project**. Major tasks are described as follows:

1. Perform site response studies for code development.
2. Develop a better understanding of large lateral and vertical permanent ground deformations associated with liquefaction, and develop corresponding simplified engineering methods.
3. Continue U.S. - Japan cooperative research in liquefaction, large ground deformation, and effects on buried pipelines.
4. Perform soil-structure interaction studies on soil-pile-structure interaction and bridge foundations and abutments, with the main focus on large deformations and the effect of ground failure on structures.
5. Study small earth dams and embankments.

This report describes the development of analytical models for the behavior of continuous pipelines subjected to permanent ground deformation. Buried steel pipelines were subjected to four idealized patterns of longitudinal permanent ground deformation and their response was determined. The pipe strains induced by these four patterns were then compared. Recommendations are provided for the design of new pipelines which must cross areas which will likely be affected by permanent ground deformation. These recommendations include increasing the pipe wall thickness, using the smallest allowable soil cover over the top of the pipe, and backfilling the pipelines trench with lighter weight soils with a low angle of shearing resistance.

ABSTRACT

The response of buried steel pipelines to permanent ground displacement is investigated. Specifically, pipeline response to four different idealized patterns of longitudinal permanent ground deformation, wherein the non–recoverable soil movement is parallel to the pipeline axis, is considered. The pipe material is assumed to be linear elastic while the force–deformation relationship of the soil–pipeline interface is taken to be elasto–plastic (elastic spring–slider) or rigid–plastic (rigid spring–slider).

The four patterns of longitudinal permanent ground deformation investigated are idealizations of patterns observed in past earthquakes. They are; (a) uniform ground strain (Ramp), (b) rigid block movement, (c) uniform ground strain with a free face (Ramp/Step) and (d) symmetric uniform ground strain (Ridge). For the first two patterns, the exact response is determined and compared with a simplified model which neglects the elastic portion of the force–deformation relationship at soil–pipeline interaction. It is found that the simplified models predict maximum pipeline strains within 5 percent of the exact values. For the third and fourth patterns of longitudinal permanent ground deformation, results are presented for the simplified interface model (rigid spring–slider) only.

TABLE OF CONTENTS

TABLE OF CONTENTS (Cont'd)

LIST OF ILLUSTRATIONS

LIST OF ILLUSTRATIONS (Cont'd)

LIST OF ILLUSTRATIONS (Cont'd)

LIST OF TABLES

LIST OF TABLES (Cont'd)

SECTION I
INTRODUCTION

The integrity of buried pipelines is a major concern for designers, owners, and users. The public depends on pipelines to supply gas, oil and water, and for waste removal. Thus pipelines are the veins and arteries of society. The failure of a pipeline can lead to economic losses, ecological damage and possible loss of life.

Observed seismic damage to buried welded steel pipelines has been attributed to both wave propagation and permanent ground deformation (PGD). Seismic wave propagation damage results from axial and bending strains induced in a pipeline due to transient earthquake waves travelling along the ground surface. These strains can lead to pinhole leaks in areas previously weakened by corrosion. If the induced pipeline strains are large enough, they can cause local buckling and subsequent tearing of the pipe wall. For example, O'Rourke and Ayala [1] attribute the failure of a 42 in. diameter, x–42 grade, welded steel water pipeline in Mexico City to seismic wave propagation caused by the 1985 Michoacan earthquake.

Permanent ground deformation refers to nonrecoverable soil movement due to landslides, surface faulting, settlement, or liquefaction induced lateral spreading. Herein we restrict our attention to landslides and liquefaction induced lateral spreading. The response of a buried pipeline to this type of PGD is a function of the pipeline orientation with respect to the direction of ground movement. In general, a pipeline would be exposed to some combination of transverse PGD and longitudinal PGD. For transverse PGD the soil movement is perpendicular to the pipeline axis, while for longitudinal PGD the soil movement is parallel to the pipeline axis. This type of movement can result in pipeline failure. For example O'Rourke and Tawfik [2] describe damage to five steel pipelines near the Upper Van Norman Reservoir due to transverse PGD resulting from the 1971 San Fernando earthquake.

In this report, the response of linear elastic steel pipe to various idealized patterns of longitudinal PGD is determined. In section 2, existing information on the magnitude and spatial extent of liquefaction induced lateral spreading is briefly presented In addition, observed PGD patterns are reviewed and the four idealized patterns of longitudinal PGD considered herein are identified. A model for the force deformation relationship at the soil pipe interface is presented in Section 3. In Section 4, the axial strain in a pipeline

subjected to a uniform ground strain (Ramp) pattern of longitudinal PGD is presented. The pipe strain is evaluated using an elastic spring–slider developed in Section 3 to model the soil–pipe interface as well as a simplified model in which the spring portion of the spring–slider is assumed rigid. In Section 5, pipeline axial strain is evaluated for a rigid block pattern of longitudinal PGD. Again, both the complete soil pipeline interfaces model (elastic spring–slider) as well as a simplified model (rigid spring–slider) are used. In Section 6 pipeline axial strain resulting from uniform ground strain with a free face (Ramp/Step) longitudinal PGD patterns is presented. In this section, results are presented only for the simplified interface model (rigid spring–slider). A symmetric uniform strain (Ridge) PGD pattern is investigated in Section 7 using the simplified interface model. Section 8 presents a comparison between the pipeline strains induced by the four idealized PGD patterns. A summary and the recommendations from the study are presented in Section 9.

SECTION 2
PERMANENT GROUND DISPLACEMENT

The strain induced in a buried pipeline is a function of the PGD magnitude, the spatial extent of the PGD zone and the pattern of ground movements along the pipeline route. In this section, existing techniques for estimation of the magnitude of PGD are reviewed. Information on the spatial extent of longitudinal PGD zones is also presented. In addition, observed patterns of PGD are reviewed. Finally, four idealizations of observed PGD patterns are identified. The response of a buried pipeline subjected to these idealized patterns is determined in Section 4 through 7.

2.1 PGD Magnitude

Modeling PGD due to liquefaction induced lateral spreading is an area of ongoing research. In his state of the art report, Finn [3] summarizes some of the more important contributions. He cites work by Hamada, Yasuda, Isoyama and Emoto [4] which suggests PGD induced by liquefaction of sandy soil is closely related to the geometrical configuration of estimated liquefiable layers. They have proposed a regression formula to predict the magnitude of horizontal PGD δ, in meters, as a function of the thickness of the liquefied layer h, in meters, and the slope θ_g, in percent, of the lower boundary of the liquefied layer or the ground surface, whichever is larger

$$\delta = 0.75 \sqrt[2]{h} \cdot \sqrt[3]{\theta_g} \tag{2.1}$$

Youd and Perkins [5] introduce the concept of a Liquefaction Severity Index (LSI) which is defined as the amount of PGD, in inches, associated with lateral spreads on gently sloping ground and poor soil conditions. LSI is arbitrarily truncated at 100. They present an empirical relationship for LSI as a function of the earthquake magnitude M_w and distance R to the site, in kilometers, for Western U.S. Earthquakes

$$\log \text{LSI} = -3.49 - 1.86 \log R + 0.98 M_w \tag{2.2}$$

Figure 2–1 shows a comparison between measured LSI and values predicted by eqn. (2.2). This relationship is not directly applicable to the Eastern U.S. since seismic wave

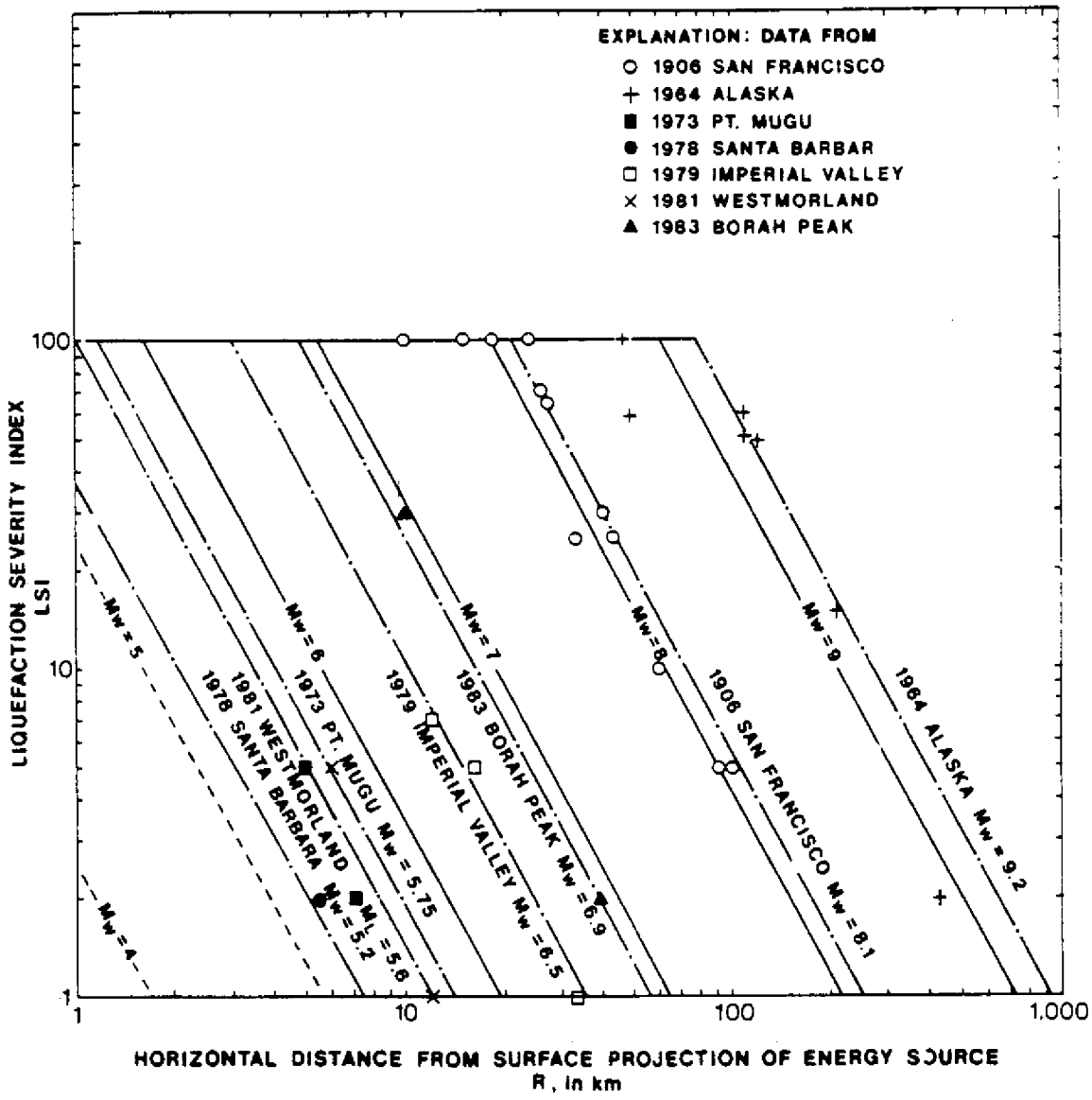

FIGURE 2-1 LSI from Several Western U.S. Earthquakes and Values Predicted by Equation 2-2 (after Youd and Perkins, 1987).

attenuation characteristics in the Western U.S. are significantly different than those in the Eastern U.S..

More recently Baziar [6] has developed an analytical relation for the magnitude of PGD, δ, for Western U.S. earthquakes based upon the Newton Sliding Block model. His relationship is

$$\delta = 2 \frac{V_{max}^2}{A_{max}} \cdot F \tag{2.3}$$

where V_{max} = peak ground velocity, A_{max} = peak ground acceleration and F is a shape factor which is a function of the ratio of the yield acceleration to the peak ground acceleration. Figure 2–2 shows a comparison between the Youd and Perkins empirical relationship for LSI = δ given by eqn. (2.2) and the Baziar analytical relationship given by eqn 2 3.

Finally, Towhata et al. [7] use a variational principle to develop an analytical relation for the magnitude of liquefaction induced PGD. Figure 2–3 shows measured horizontal PGD magnitudes in Noshiro City caused by the 1983 Nihonkai–Chubu earthquake as well as the PGD calculated by the Towaha et al. procedure.

All four methods for estimating the magnitude of PGD are the result of recent research. The authors are not in a position to recommend any particular method as being the best.

2.2 Spatial Extent of PGD Zones

As will be shown later, the length L of the lateral spread zone (i.e. spatial dimension in the direction of ground movement) is a key parameter in determining the response of buried pipeline to longitudinal PGD. Using case history data from the 1964 Niigata Earthquake and the 1983 Nihonkai Chubu Earthquake, Suzuki and Masuda [8] present empirical information on the magnitude and extent of the lateral spread zone for longitudinal PGD. Figure 2–4 shows the PGD patterns observed by Suzuki and Masuda. The upper figure shows a region of tensile ground strain while the lower figure is compressive. Figure 2–5 shows a plot of observed values of δ and L. There are a total of 290 data points in this figure. The 133 data points with positive values of δ correspond to tensile deformations as shown in Figure 2–4a. The remaining 157 data points below the $\delta = 0$ line are compressive

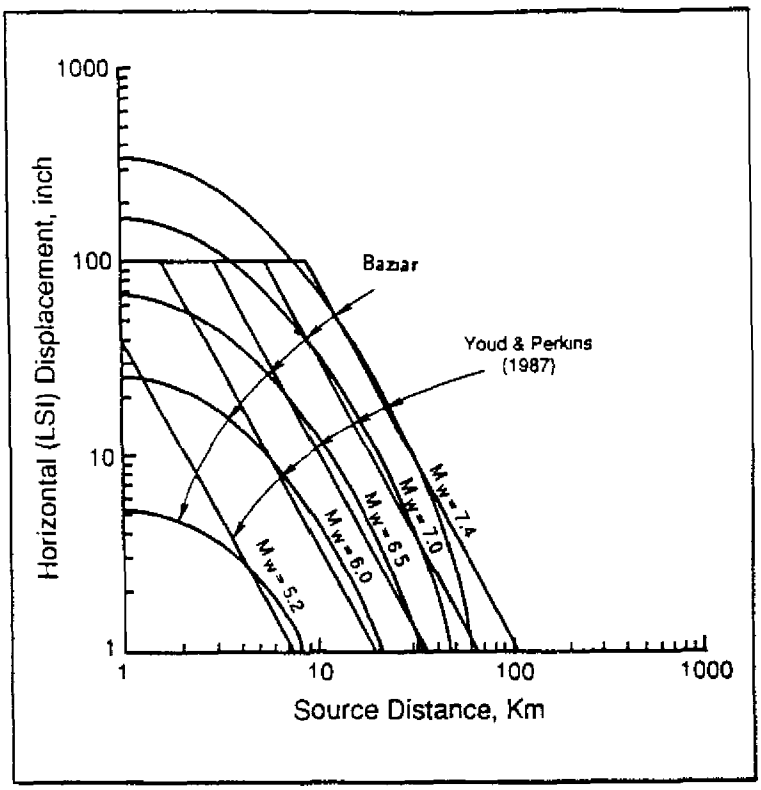

FIGURE 2-2 Comparision of Empirical LSI relationship from Youd and Perkins (1987) given by Equation 2.2 with Baziar (1991) analytical relationship given by Equation 2.3 (modified after Baziar, 1991).

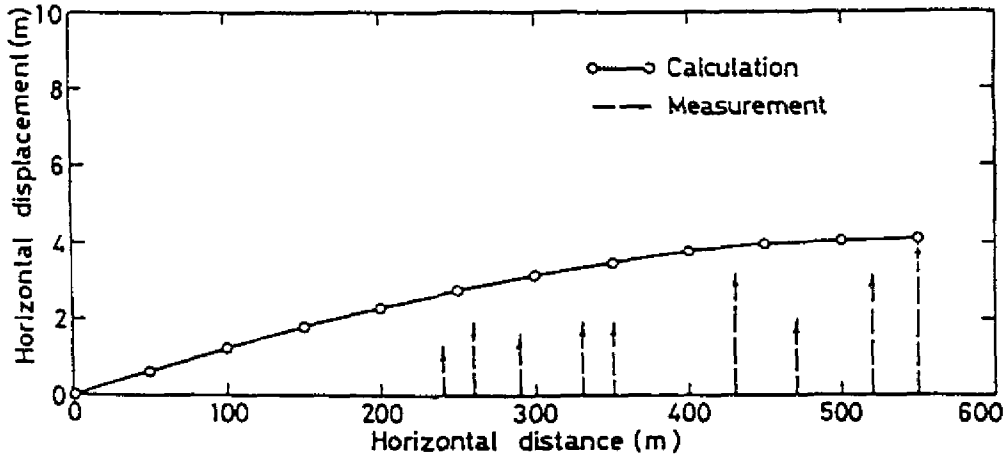

FIGURE 2-3 Measured and Calculated Horizontal Ground Movements in Noshiro City resulting from the 1983 Nihonkai-Chubu Earthquake (after Towhata et al., 1991).

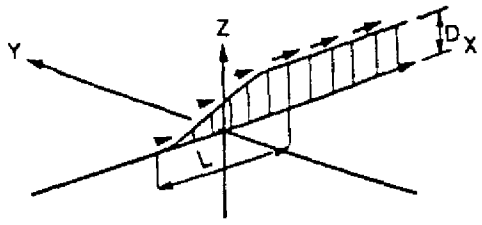

(a) Tensile Ground Strain

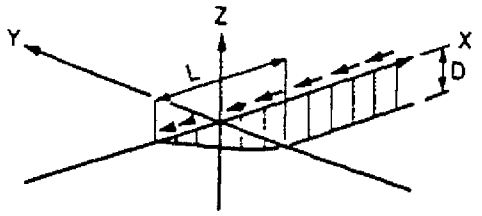

(b) Compressive Ground Strain

FIGURE 2-4 Longitudinal Permanent Ground Deformation Patterns observed by Suzuki and Masuda (1991).

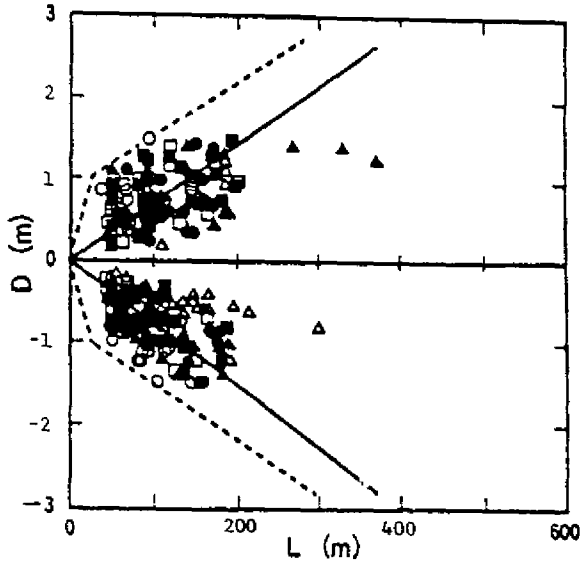

FIGURE 2-5 Empirical Data on the Magnitude $\delta = D$ for Longitudinal PGD (after Suzuki and Masuda, 1991).

deformation as shown in Figure 2–4b. Note in Figure 2–5 that $L \leq 400$ m. and $\delta \leq 1.5$ m. The average ground strain, $\alpha = \delta/L$, for both tensile and compressive deformations generally falls in the range $0.002 \leq \alpha \leq 0.03$ with typical values being 0.007 or 0.008.

2.3 Observed PGD Patterns

As will be shown later, the pattern of ground deformation (i.e. the distribution of PGD along the pipeline axis) influences the strain induced in a buried pipeline by longitudinal PGD. Towhata et al. [7] observed that vertical soil movement occasionally accompany liquefaction induced lateral spreading. In general, subsidence tends to occur in the upper portion of the slope and heaving at the lower portion. Herein, these possible vertical soil movements are neglected and buried pipe response to the horizontal component of PGD will be determined.

Hamada et al. [9] have studied PGD which resulted from liquefaction during the 1964 Niigata Earthquake and the 1983 Nihonkai–Chubu Earthquake. Figure 2–6 shows PGD observed along six section lines in Niigata City as a result of the 1964 earthquake. In this figure as well as in Figures 2–7, 2–8 and 2–9, a vertical line with an open circle indicates permanent movement to the right while a solid circle indicates movement to the left. In general, at the bank of a river the PGD is towards the river. For example Figure 2–6(c) shows PGD to the left near the right abutment of the Bandai Bridge, and PGD to the right near the left abutment. The same pattern is evident at the left bank of the Shinano River in Figure 2–6(a), the left abutment of the Showa Bridge in Figure 2–6(b), and the left abutment of the Yachiyo Bridge in figure 2–6(f). At some distance away from a river, Hamada et al. [9] note that the direction of PGD appears to be controlled by the slope of the ground surface or the slope of the bottom of the liquefied layer. For example the PGD between the Echigo line and the Niigata–Kotsu line in Figure 2–6(a) is away from the Shinano River because the lower boundary face of the liquefied layer falls away from the river at that location. Figure 2–7 shows PGD observed along twenty–seven section lines in Noshiro City as a result of the 1983 Nihonkai–Chubu Earthquake.

As shown in Figure 2–6 and 2–7, the observed patterns of longitudinal PGD can be quite complex. However for some of these case histories, the observed patterns can be idealized. For example in Figure 2–6(e), there is a fairly linear variation of PGD with distance from the right, resulting in a displacement of roughly 3.5 m. about 350 m. to the left of the point of zero PGD. This corresponds to an average ground strain $\alpha = \delta/L$ of roughly 0.01 over

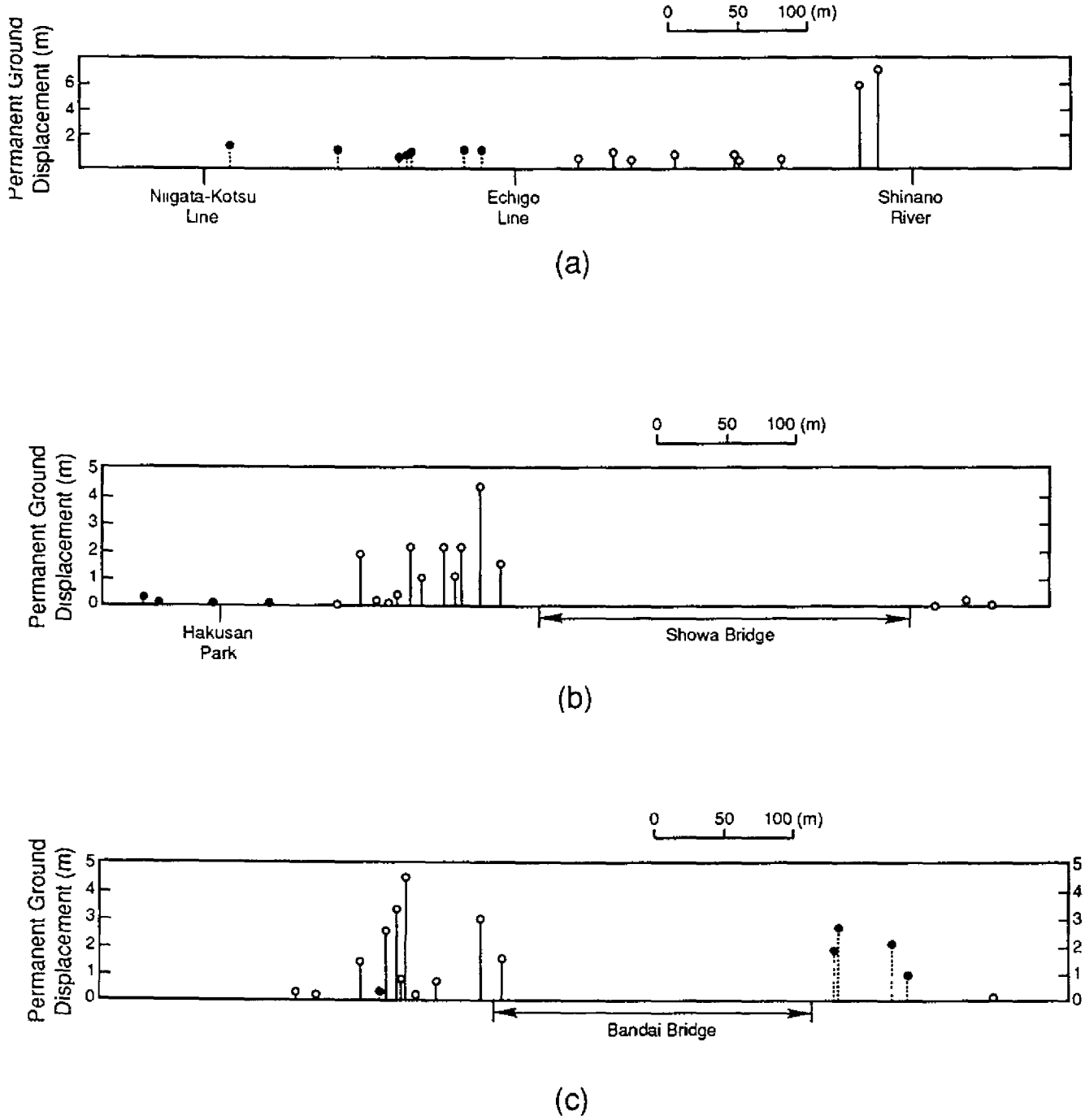

FIGURE 2-6 PGD patterns observed in Niigata City after the 1964 Niigata Earthquake, solid circle indicates movemen to the left, open circle indicates movement to the right (after Hamada et al. 1986).

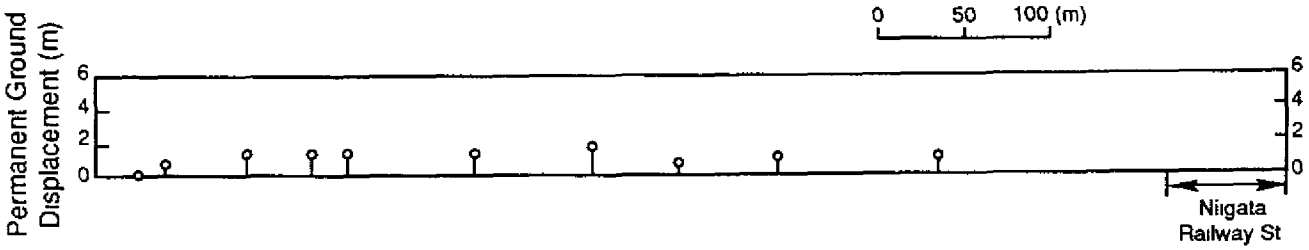

(d)

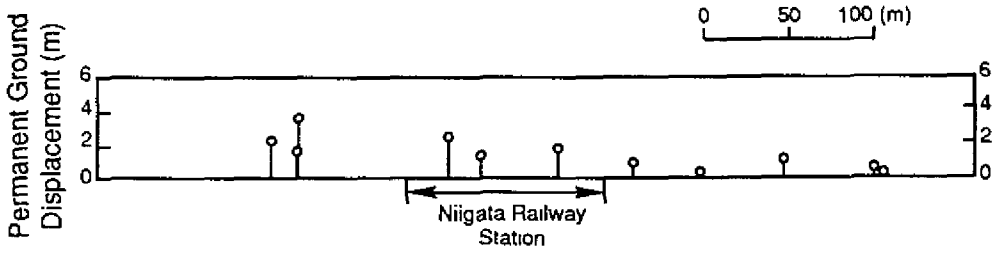

(e)

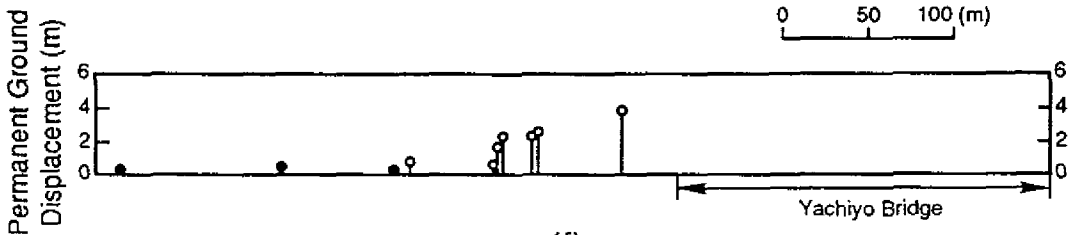

(f)

FIGURE 2-6 (continued)

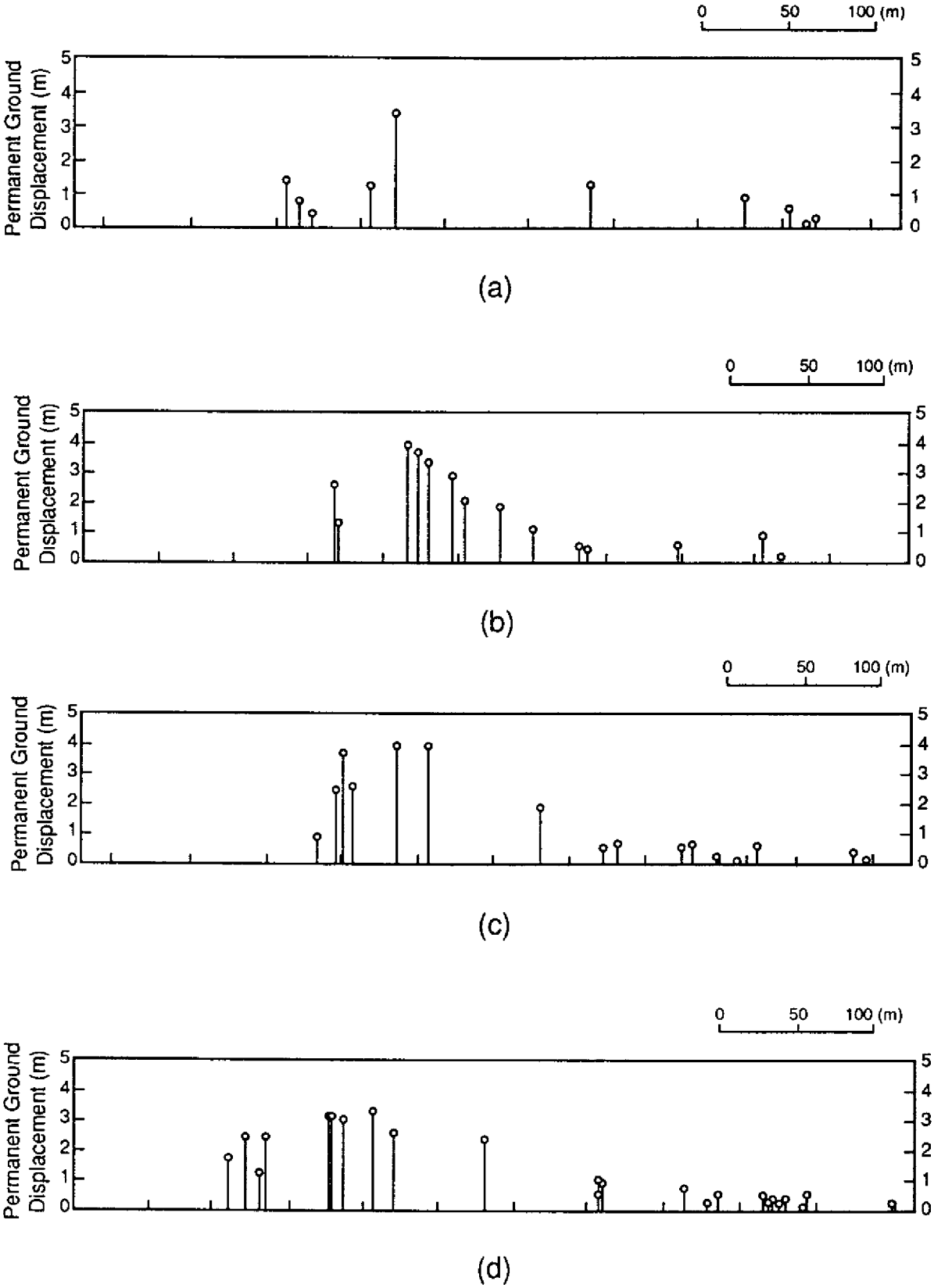

FIGURE 2-7 PGD patterns observed in Noshiro City after the 1983 Nihonkai-Chubu Earthquake (after Hamada et al., 1986).

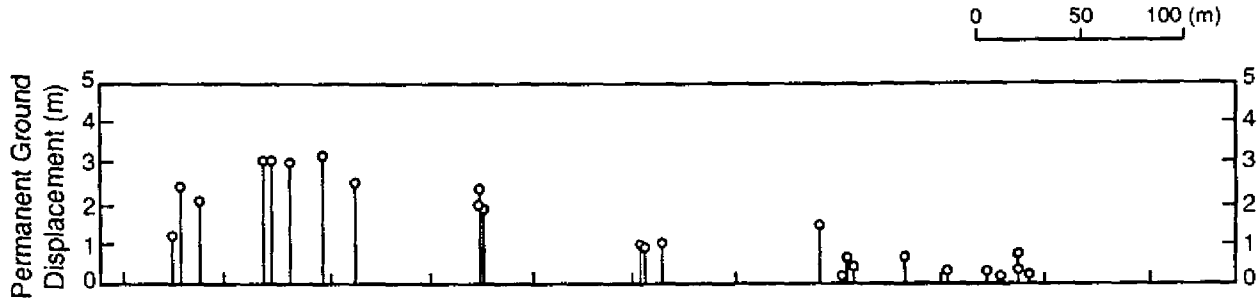

(e)

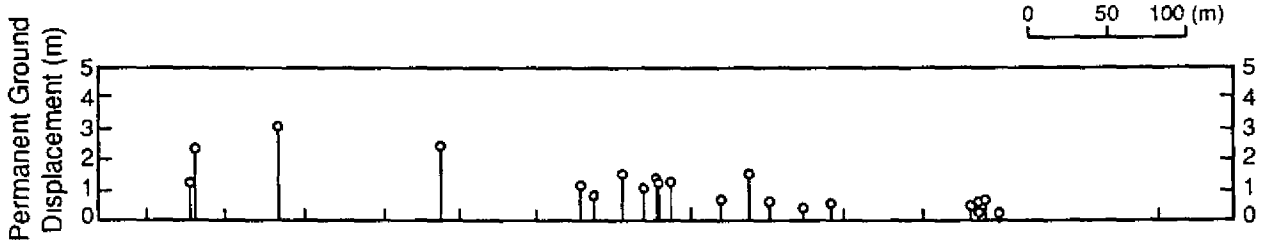

(f)

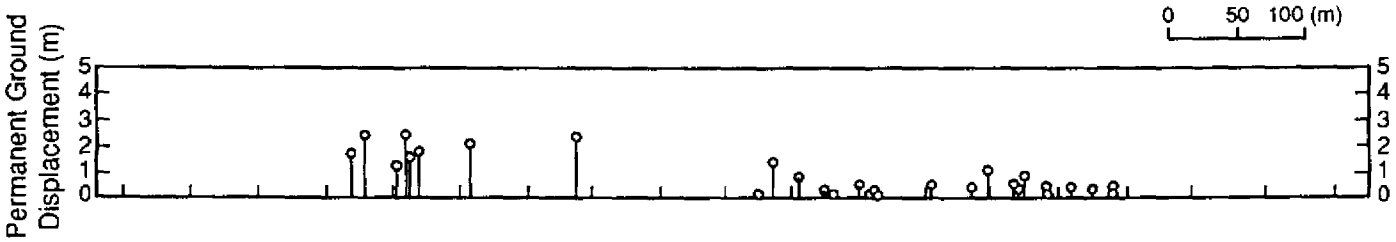

(g)

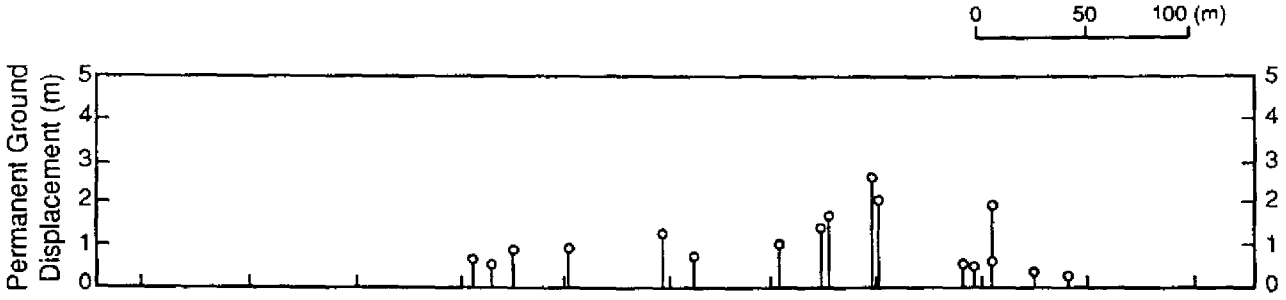

(h)

FIGURE 2-7 (continued).

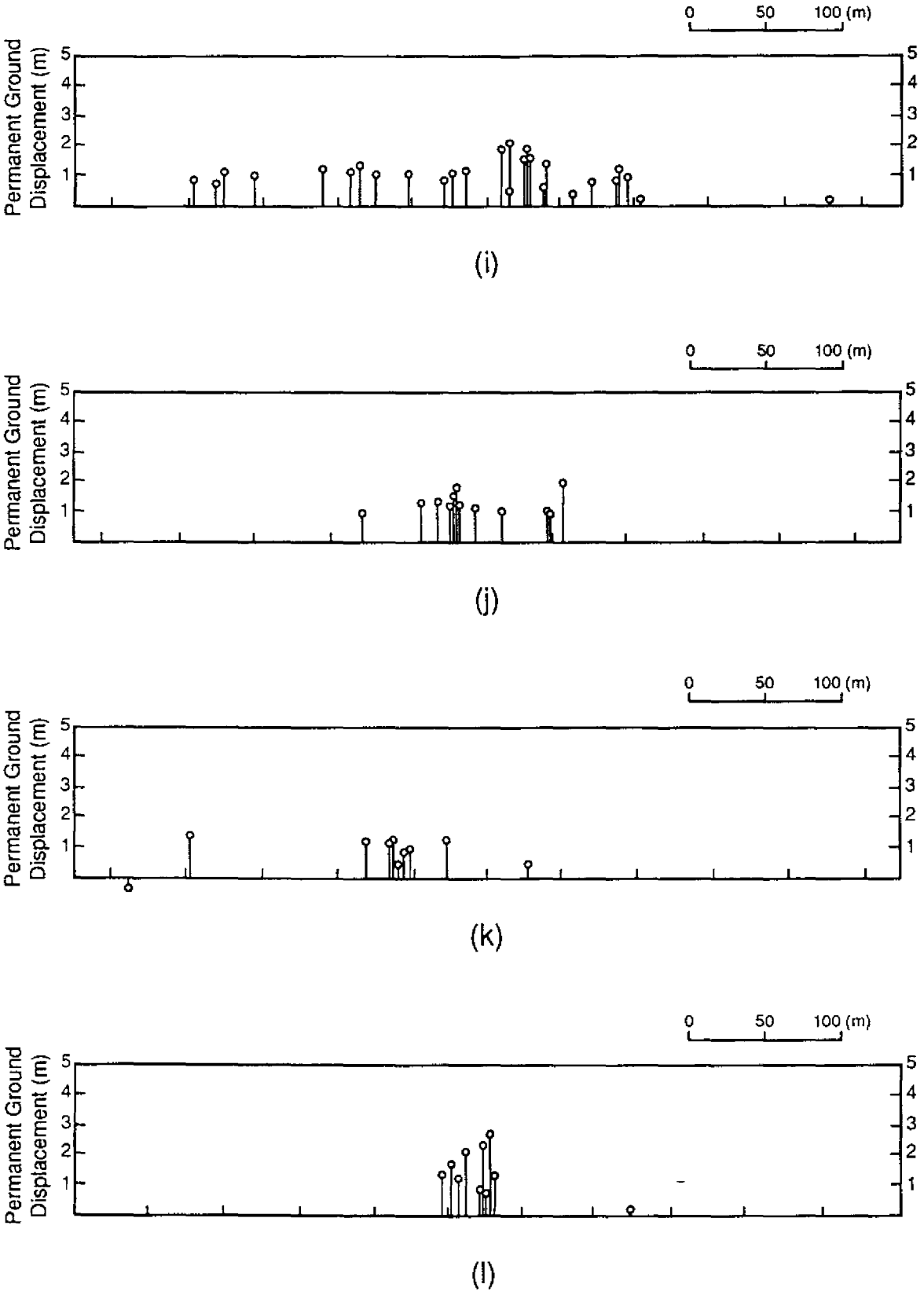

FIGURE 2-7 (continued)

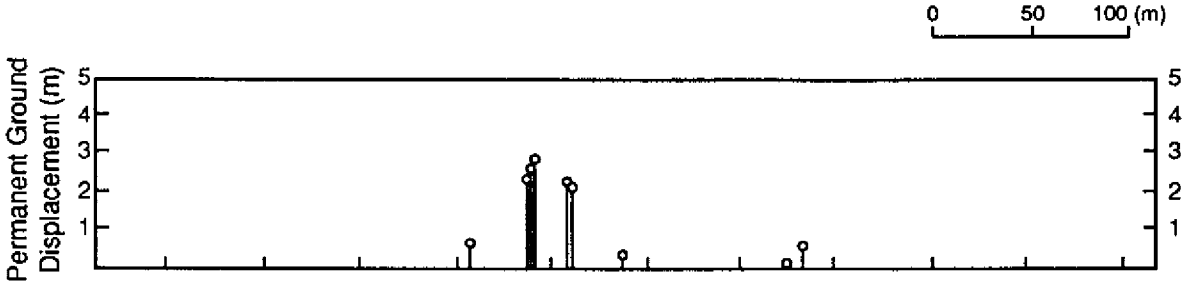

(m)

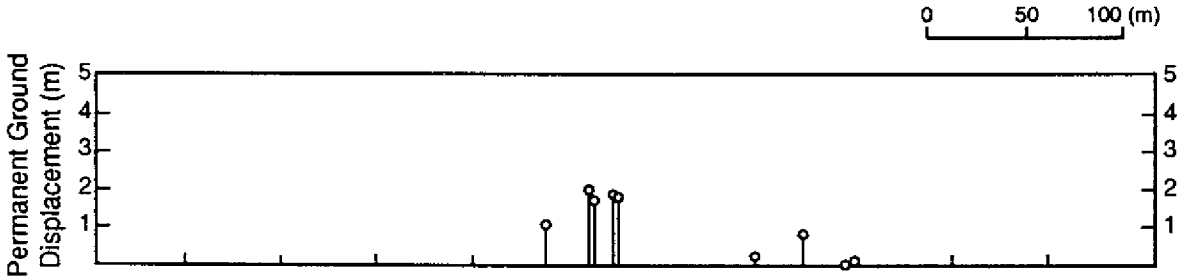

(n)

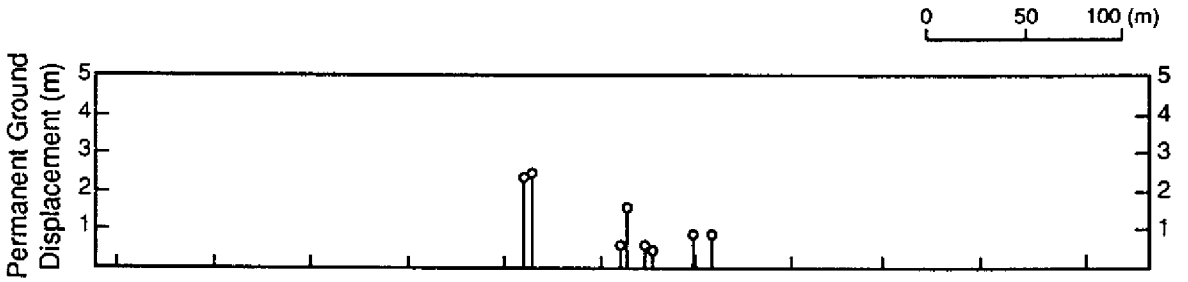

(o)

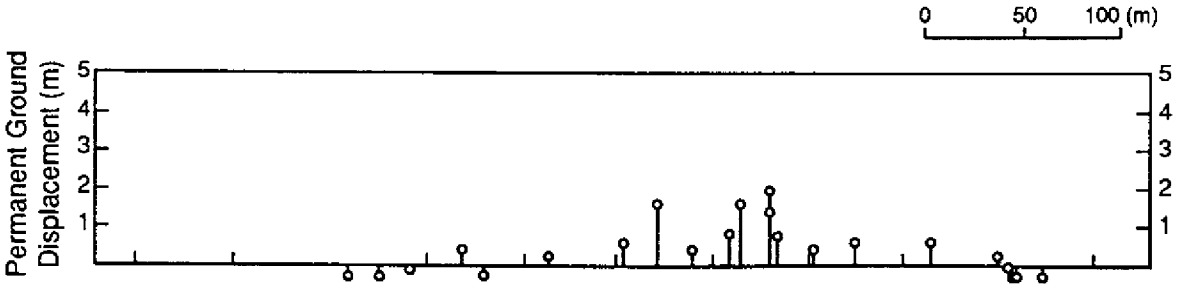

(p)

FIGURE 2-7 (continued)

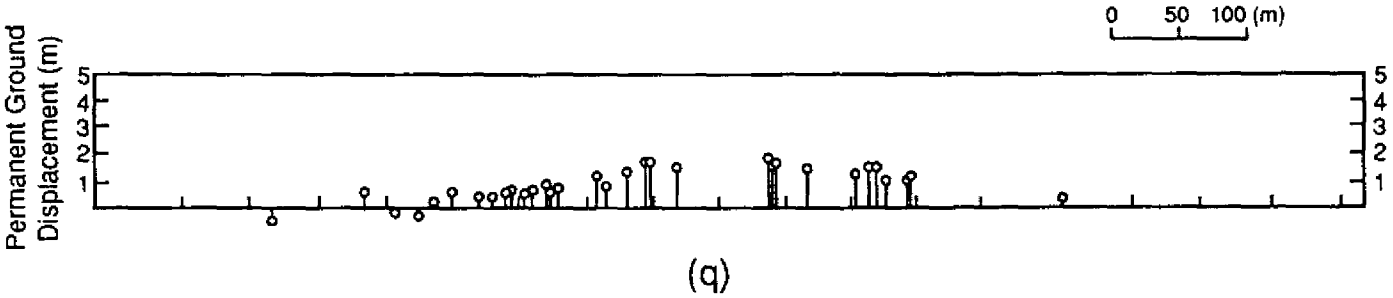

(q)

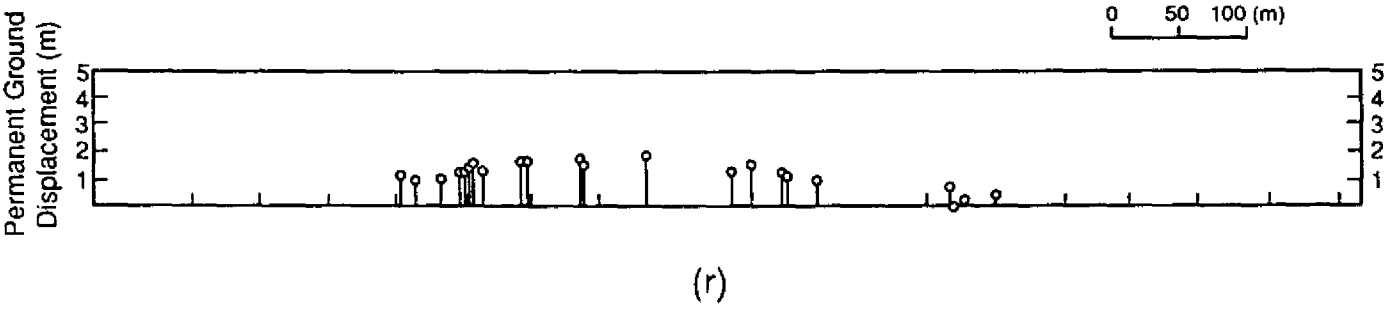

(r)

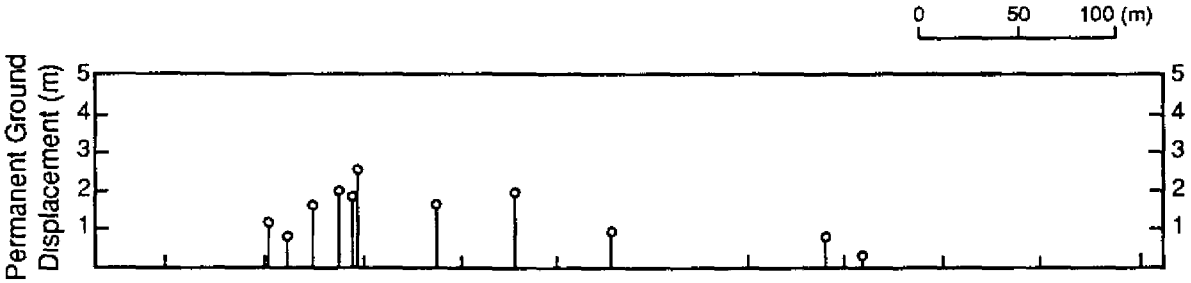

(s)

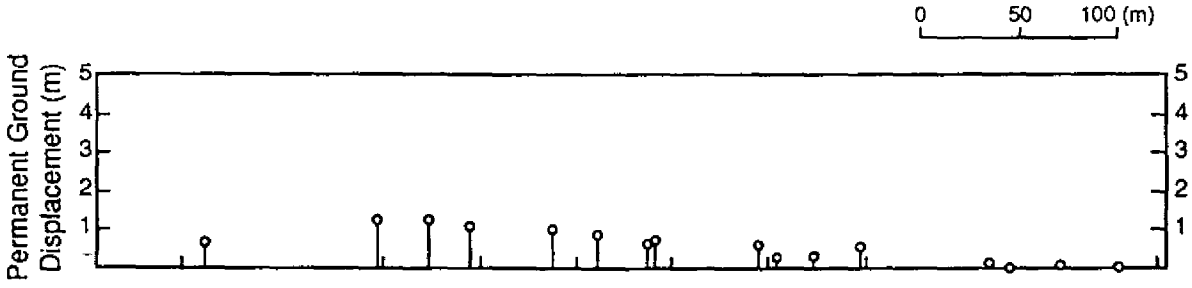

(t)

FIGURE 2-7 (continued)

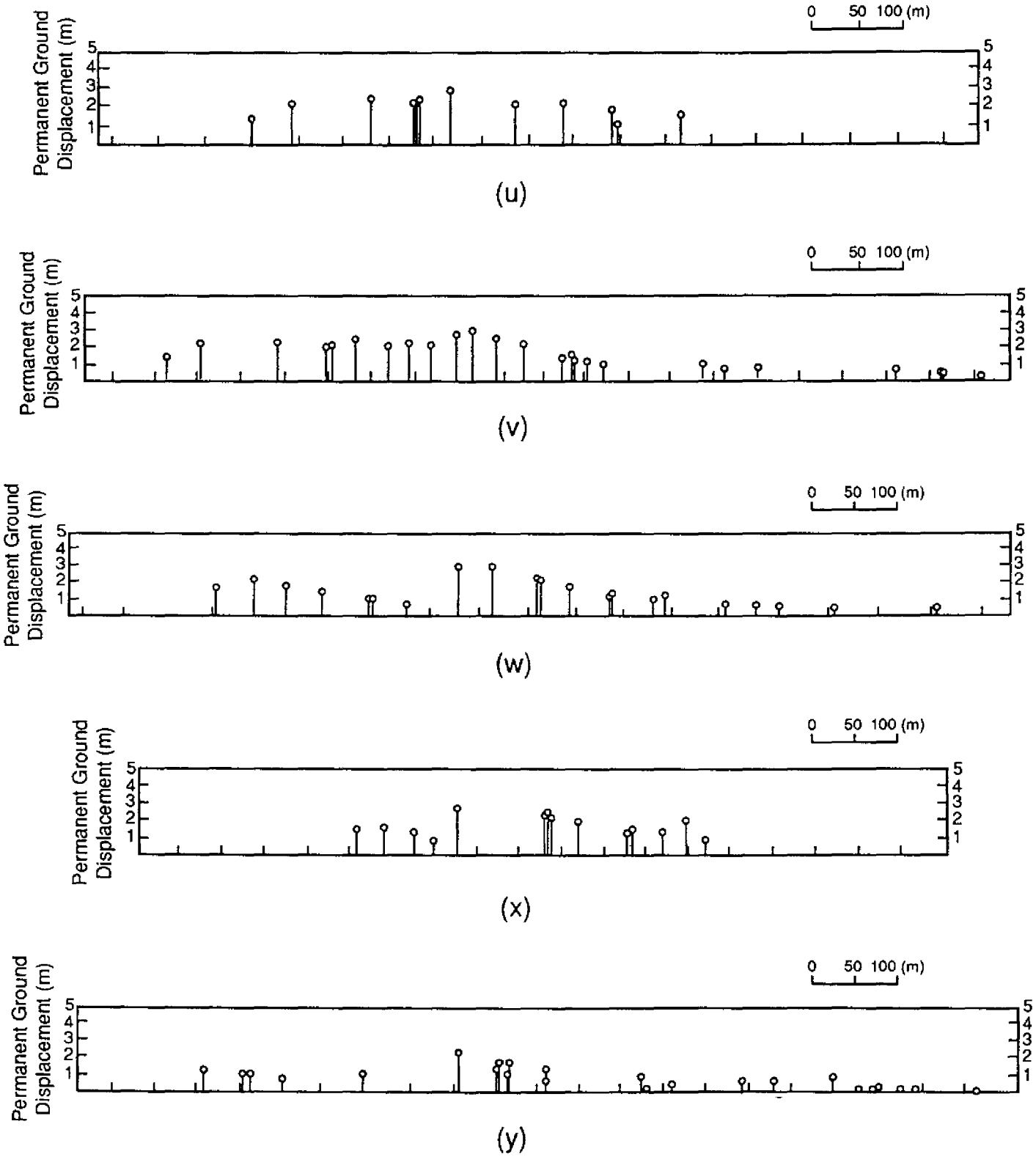

FIGURE 2-7 (continued)

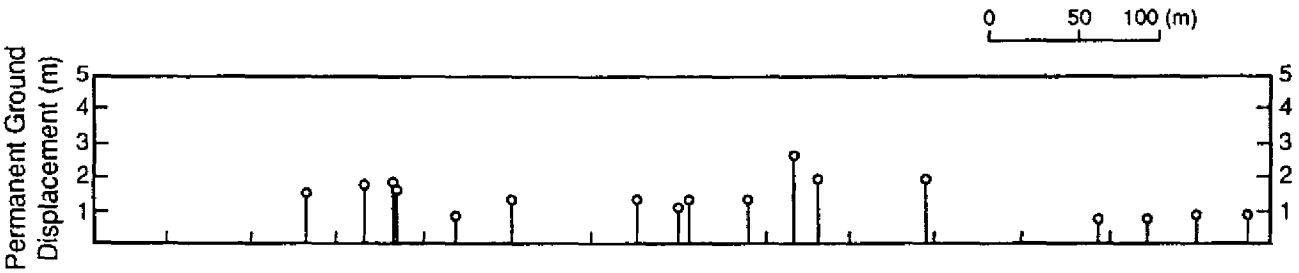

(z)

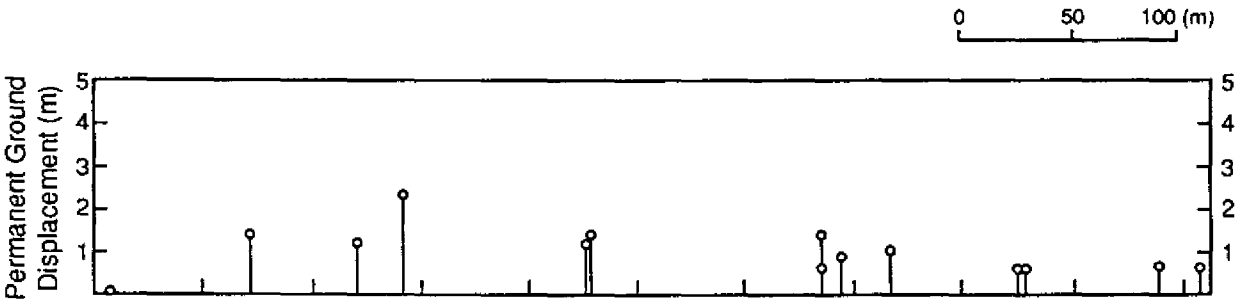

(aa)

FIGURE 2-7 (continued)

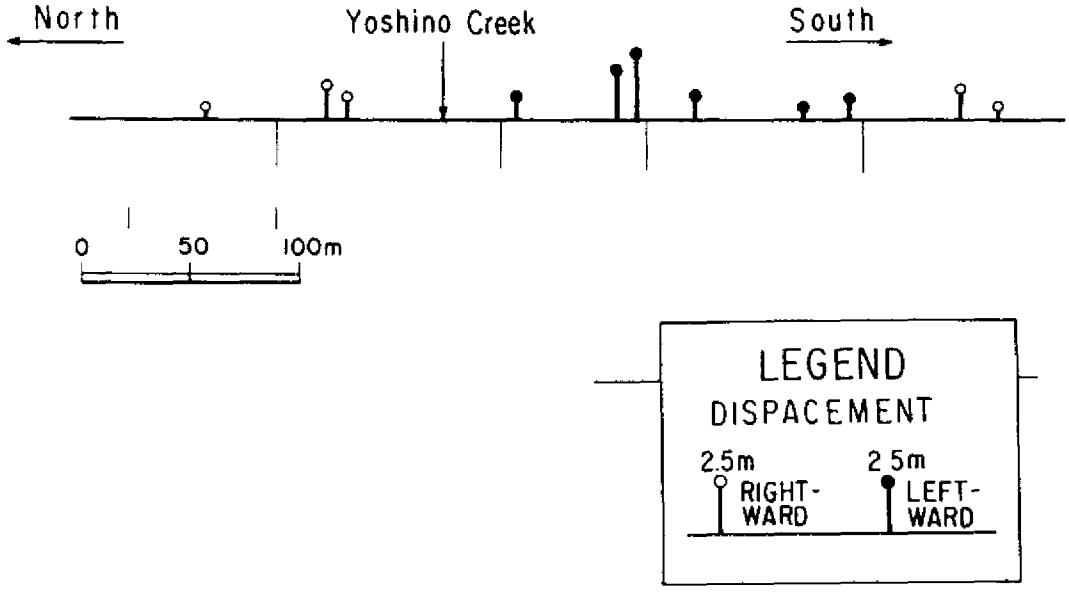

FIGURE 2-8 PGD pattern observed near the Yoshino Creek in Fukui City after the 1948 Fukui Earthquake (after Hamada, Wakamatsu and Yasuda, 1989).

the length L of 350 m. A somewhat similar pattern can be observed at the far left hand side of Figure 2–6(d) when a displacement of roughly 2.0 m. occurs about 60 m to the right of the zero PGD point. This corresponds to an average ground strain of roughly 0.033 over a distance of 60 m.

Other examples of fairly linear variation of PGD with distance were observed in Noshiro City. In Figure 2–7(a), the maximum PGD is roughly 3.5 m, while about 250 m. to the right the PGD is zero. This results in an average ground strain of 0.014. In the center of Figure 2–7(b), the maximum PGD is roughly 4 m. but about 140 m. to the right it's zero, resulting in a ground strain of about 0.029. Finally, towards the center of Figure 2–7(s), the maximum PGD is roughly 2.5 m and there is no PGD about 280 m. to the right, leading to an average ground strain of 0.009.

Some of the other case histories for Noshiro City show relatively uniform PGD over various distances. For example the observed PGD in Figure 2–7(j) has a relatively constant value of roughly 1.5 m. over a distance of roughly 130 m. Similarly in Figure 2–7(u), the observed PGD is almost a constant value of 2 m. over a distance of roughly 500 m.

Hamada, Wakamatsu and Yasuda [10] have investigated observed PGD due to liquefaction occasioned by the 1948 Fukui Earthquake. Figure 2–8 shows PGD near the Yoshino Creek in the Western part of Morita–cho. The PGD in Figure 2–8 follows the trend noted previously, that is, at each side of the creek the ground movement was towards the creek. The maximum PGD was about 3 m. and occurred about 85 m. to the right of the creek. The ground movement on either side of this maximum PGD point decrease in roughly a linear fashion, being about zero immediately to the right of the creek and about zero roughly 190 m. to the right of the creek. The corresponding ground strain on either side of the point of maximum PGD is roughly 0.035. The ground deformation is tensile to the right of the point of maximum PGD,and compressive to the left.

On the left hand side of Figure 2–8 the maximum PGD was about 2 m in a direction towards the creek and occurred about 60 m to the left of the creek. The PGD on either side of this local maximum decrease in roughly a linear fashion, being about zero immediately to the left of the creek and about zero roughly 120 m to the left of the creek. The corresponding ground strain on either side of this local maximum PGD is roughly 0.033, being tensile to the left and compressive to the right.

A final example of observed PGD is the area between the Ohgata Elementary School and the Tsusen River in Niigata City which was investigated by Yasuda et al. [11]. Figure 2–9 shows PGD that resulted from the 1964 Niigata Earthquake. In the center of this figure, the PGD was towards the river, as one might expect based on the trend previously noted herein. The maximum PGD is roughly 7.5 m and occurs roughly 210 m to the left of the Ohgata School. Between the school and the point of maximum PGD, there is a fairly linear variation of PGD with distance from the point of zero PGD at the school. This corresponds to an average tensile ground strain of roughly 0.036.

There are only two data points in Figure 2–9 between the maximum PGD location in the center of the figure and the Tsusen River on the left. Figure 2–10 shows the idealized horizontal soil displacement within 210 m of the Ohgata school and three possible soil displacement patterns over the 180 m distance to the right of the river.

2.4 Idealized PGD Patterns

In subsequent sections, the axial strain in a buried pipeline subject to four idealized patterns of longitudinal PGD will be determined. These four idealized patterns are based upon the observed PGD patterns mentioned above. They are: (a) Ramp PGD, (b) Rigid Block PGD, (c) Ramp/Step PGD and (d) Ridge PGD.

2.4.1 Ramp PGD

The first idealized longitudinal PGD pattern considered herein is Ramp PGD. This corresponds to uniform ground strain α over a length L as shown in Figure 2–11. The ground strains on either side of the transition zone are zero. The soil displacement to the left of the transition zone is zero while the soil displacement to the right of the transition zone have a constant value of $\delta = \alpha L$.

The Ramp PGD pattern approximates the patterns quantified by Suzuki and Masuda [8] and shown in Figure 2–4. It also approximates the PGD pattern shown on the far left hand side of Figure 2–6(d) and towards the center of Figure 2–7(q). The Ramp pattern would be an appropriate model for the PGD shown in Figure 2–6(e) if the soil displacements on the left hand side of the figure have a constant value of about 3.5 m.

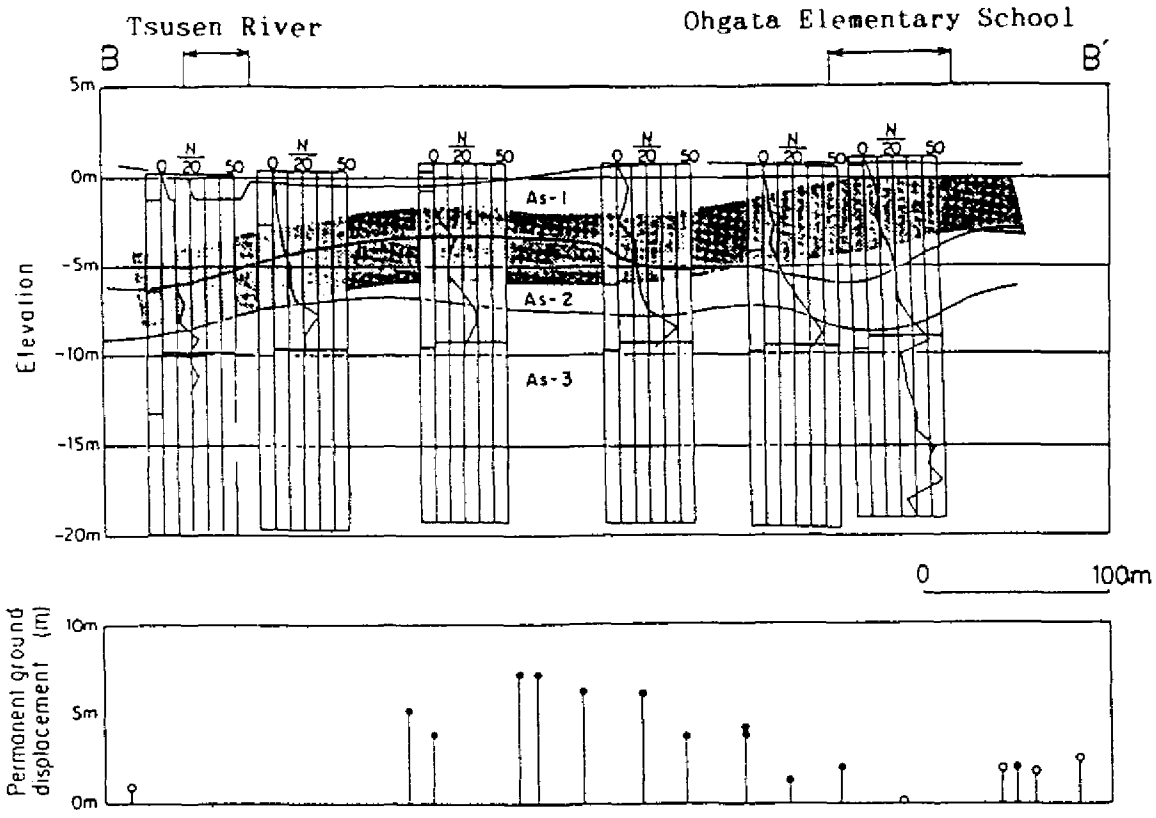

FIGURE 2-9 Permanent Ground Deformation Between the Ohgata Elementary School and the Tsusen River in Niigata City as Result of the 1964 Niigata Earthquake (after Yasuda et al. [10]).

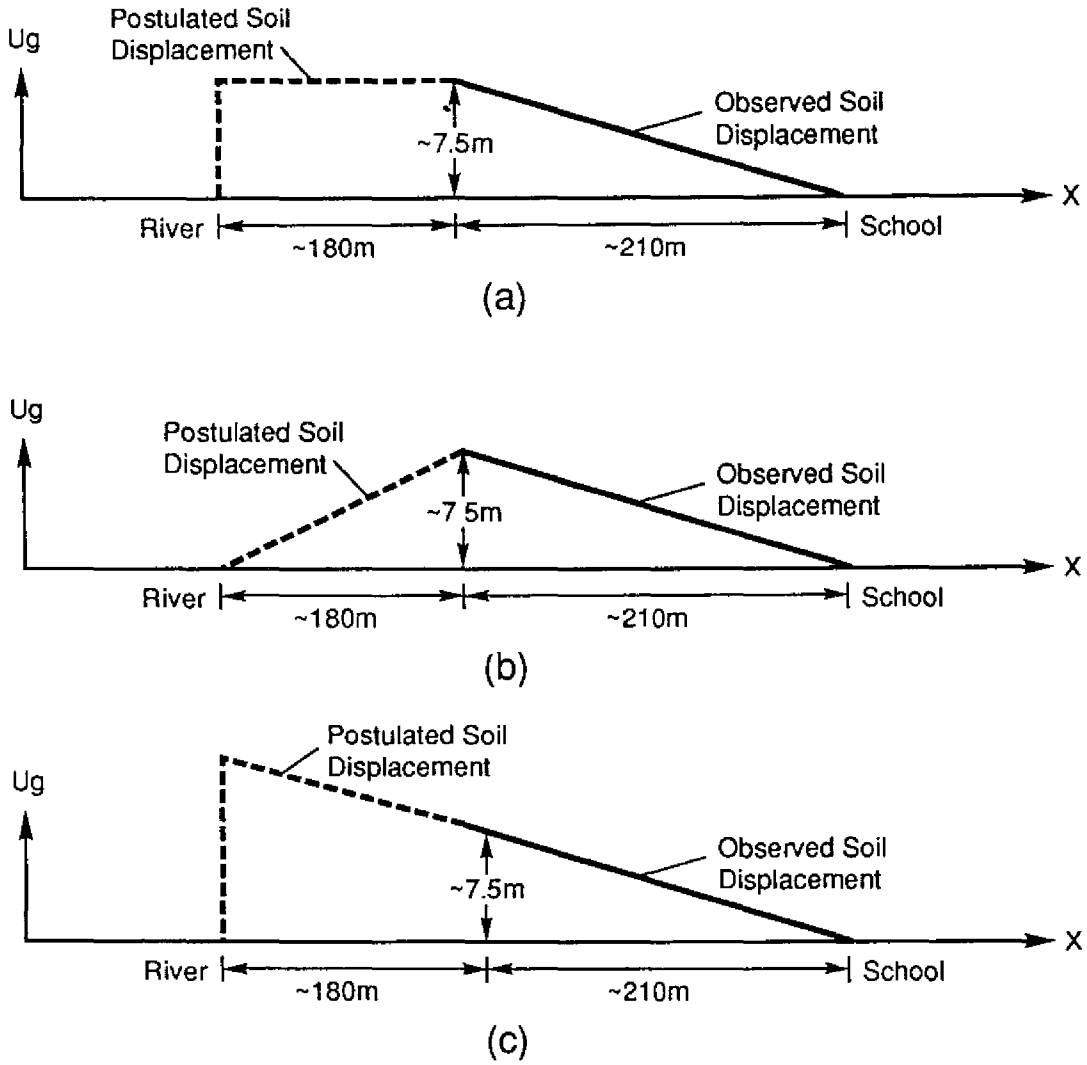

FIGURE 2-10 Idealized and Postulated Soil Displacement Patterns between the Ohgata School and the Tsusen River, (a) Combination Ramp and Ridge Block, (b) Ridge, (c) Ramp/Step.

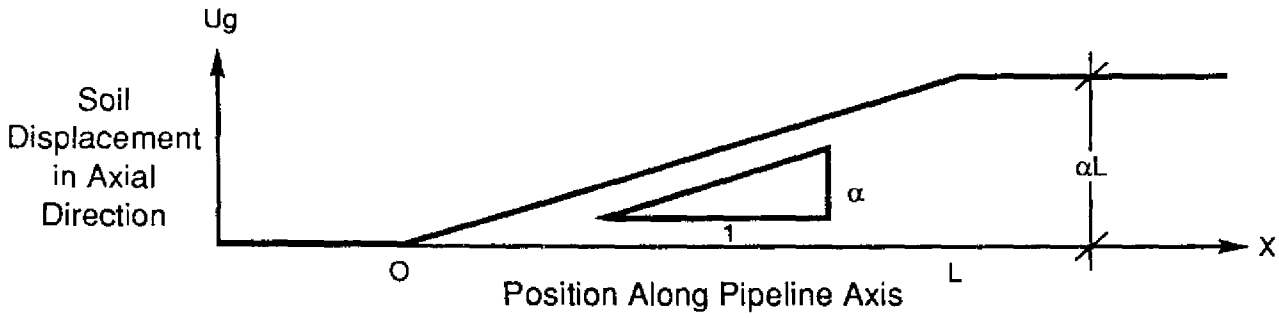

FIGURE 2-11 Idealized Ramp pattern of Longitudinal PGD.

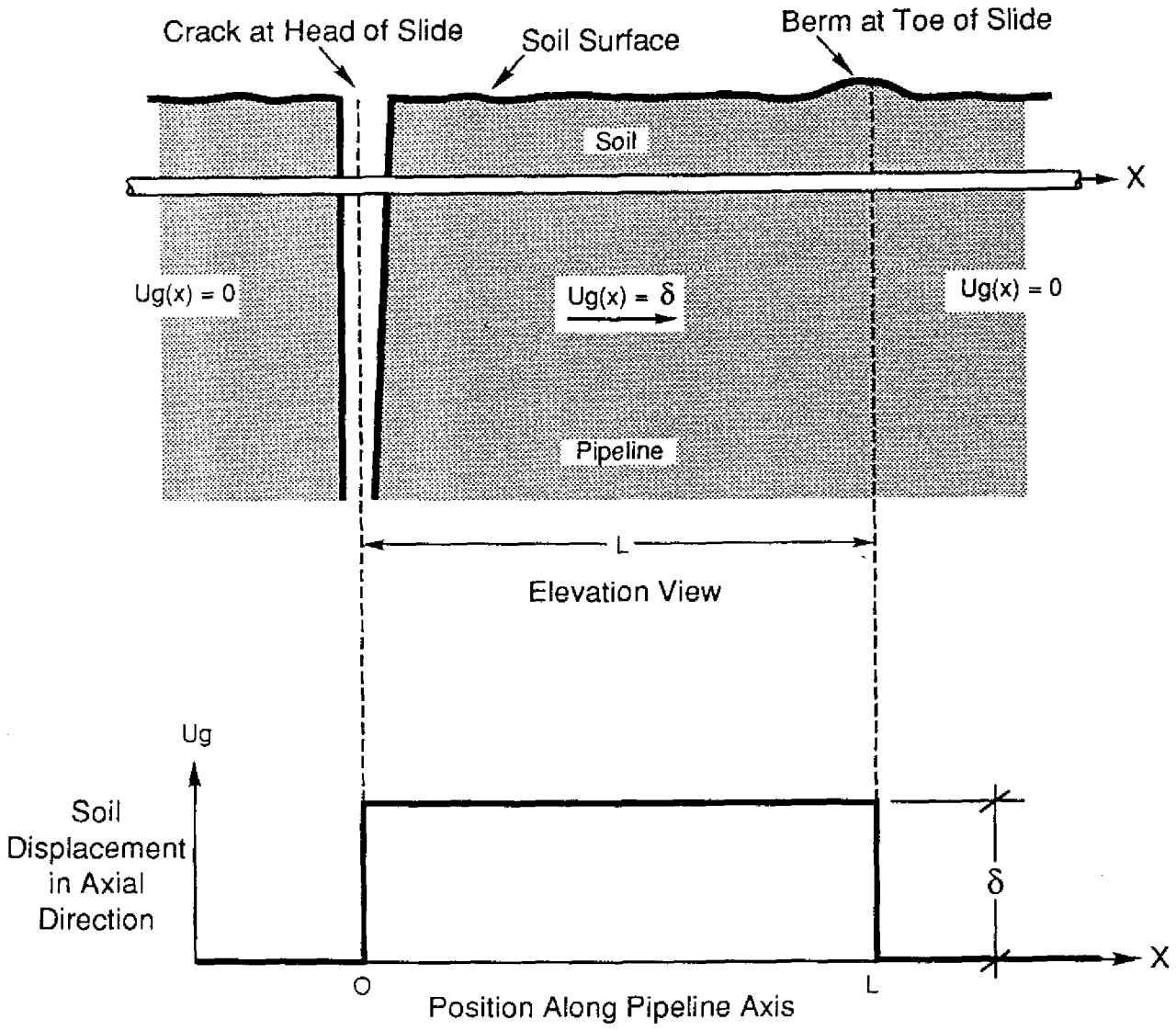

FIGURE 2-12 Idealized Rigid Block pattern of Longitudinal PGD.

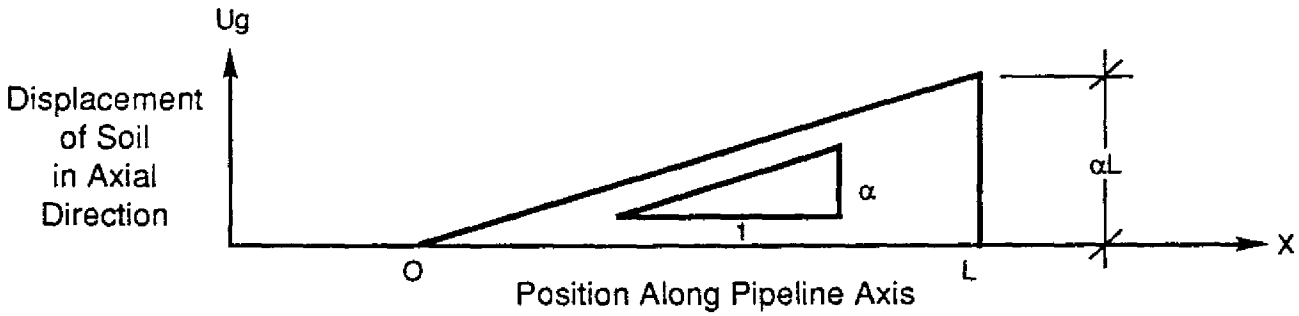

FIGURE 2-13 Idealized Ramp/Step pattern of Longitudinal PGD.

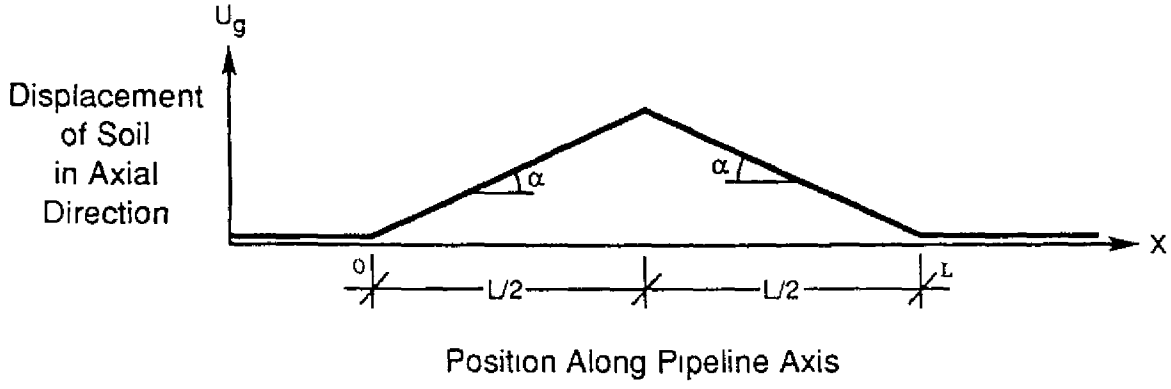

FIGURE 2-14 Idealized Ridge pattern of Longitudinal PGD.

Establishing a coordinate system with an origin at the boundary between the stable soil region (zero PGD) and the transition zone, the assumed horizontal soil displacement, $u_g(x)$, for Ramp PGD become

$$u_g(x) = \begin{cases} 0 & x < 0 \\ \alpha x & 0 < x < L \\ \alpha L & x > L \end{cases} \tag{2.4}$$

Axial pipeline strain induced by Ramp PGD is determined in Section 4.

2.4.2 Rigid Block PGD

The second idealized longitudinal PGD pattern considered herein is Rigid Block PGD. This corresponds to a mass of soil having length L, moving as a rigid body down a slight incline as shown in Figure 2–12. The soil displacement and soil strain at either side of the landslide or lateral spread zone are zero, while the displacement of the soil within lateral spread zone is a constant value δ. A ground crack or gap occurs at the head of the slide and a compression mound or berm at the toe.

The idealized Rigid Block pattern would be an appropriate model for the PGD in Figures 2–7(j) and 2–7(u) if the ground displacements on the left and right sides of these figures were zero. Establishing a coordinate system with an origin at the head of the lateral spread zone, the assumed horizontal ground displacements for Rigid Block PGD are given by

$$u_g(x) = \begin{cases} 0 & x < 0 \\ \delta & 0 < x < L \\ 0 & x > L \end{cases} \tag{2.5}$$

Axial pipeline strain induced by Rigid Block PGD is determined in Section 5.

2.4.3 Ramp/Step PGD

The third idealized PGD pattern considered herein is Ramp/Step PGD shown in Figure 2–13. This pattern could result from lateral spreading near a free face such as a

river. Soil displacement and soil strain are both zero on either side of the lateral spread zone, while the soil strain within the zone has a constant value of α.

The Ramp/Step PGD pattern would be an appropriate model for the ground movements on the right hand side of Figure 2–6(c) if the ground displacements under the BandaiBridge were zero, for the ground displacements in Figure 2–7(c) and Figure 2–7(o) if the ground displacements to the left were zero, and for the postulated pattern shown in Figure 2–10(c). Establishing a coordinate system with an origin at the beginning of the ramp, the assumed horizontal ground displacements for Ramp/Step PGD are given by

$$u_g(x) = \begin{cases} 0 & x < 0 \\ \alpha\, x & 0 < x < L \\ 0 & x > L \end{cases} \tag{2.6}$$

2.4.4 Ridge PGD

The fourth idealized pattern considered herein is Ridge PGD as shown in Figure 2–14. Soil displacement and soil strain are zero outside the zone of lateral spreading. Within the lateral spread zone, there is uniform tensile ground strain, α, to the left of the ridge (i.e. the point of maximum ground movement) and uniform compressive ground strain, α, to the right of the ridge.

The Ridge PGD pattern might be an appropriate model for the observed ground movement to the left of the Bandai Bridge in Figure 2–6(c), for the pattern in Figure 2–7(b), for the south side of the Yoshino Creek in Figure 2–8 and the postulated pattern shown in Figure 2–10(b). Establishing a coordinate system with an origin at the left side of the lateral spread zone, the assumed horizontal ground displacements for Ridge PGD are

$$u_g(x) = \begin{cases} 0 & x < 0 \\ \alpha\, x & 0 < x < L/2 \\ \alpha(L-x) & L/2 < x < L \\ 0 & x > L \end{cases} \tag{2.7}$$

Pipeline axial strain induced by Ridge PGD is determined in Section 7.

SECTION 3
SOIL – PIPELINE INTERACTION

The stress and strain in a buried pipeline subject to pseudo–static PGD are due to forces at the soil–pipeline interface. For longitudinal PGD, the key relationship is that between the force at the soil–pipeline interface and the relative displacement between the pipe and surrounding soil (i.e. direction of force and displacement parallel to the pipeline axis). The American Society of Civil Engineers Committee on Gas and Liquid Fuel Lifelines [12] suggests the use of elasto–plastic or hyperbolic models for this relationship. For simplicity, the elasto–plastic model (i.e. elastic spring–slider model) shown in Figure 3–1 is adopted herein.

Tests performed by Colton et al. [13] on a full–scale pipe placed in a trench and backfilled with cohesionless soil, indicate that the axial force/displacement relationship is linear at small displacements. The soil force reaches a "plateau" when slippage of the pipe with respect to the soil occurs. In the plateau or plastic region, the force per unit length exerted on the pipe is a constant value f_m. This is illustrated in Figure 3–2, which shows the relationship between the axial force per unit length at the soil/pipeline interface, and the relative axial displacement between the soil and pipeline.

The elasto–plastic model shown in Figure 3–2 is fully defined by two parameters. These are the maximum axial force per unit length at the soil/pipeline interface, f_m, and the axial stiffness of the soil spring, k. The relative displacement at which slippage occurs, D_s, is simply the ratio f_m/k. Characteristics of these spring–sliders are determined in this section after review and synthesis of the existing literature.

3.1 Maximum Axial Force Per Unit Length

For the case where the pipeline trench is backfilled with cohesionless soil, the ultimate force per unit length at the soil/pipeline interface, f_m, is simply the product of the coefficient of friction and the average of the vertical and horizontal forces on the pipeline, that is:

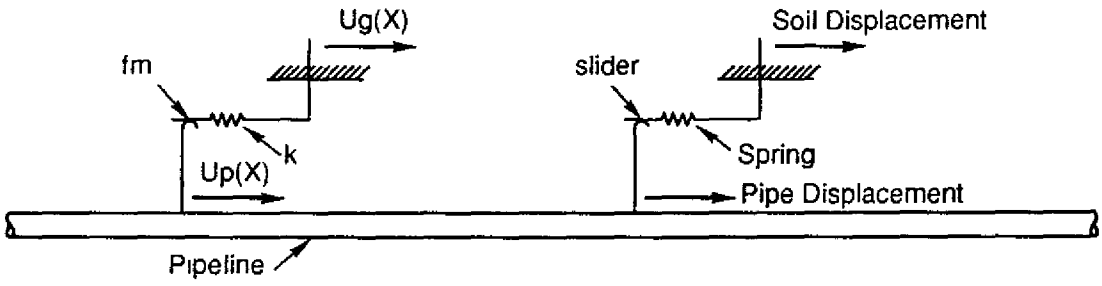

FIGURE 3-1 Spring/Slider Model for Axial Soil-Pipeline Interface Forces.

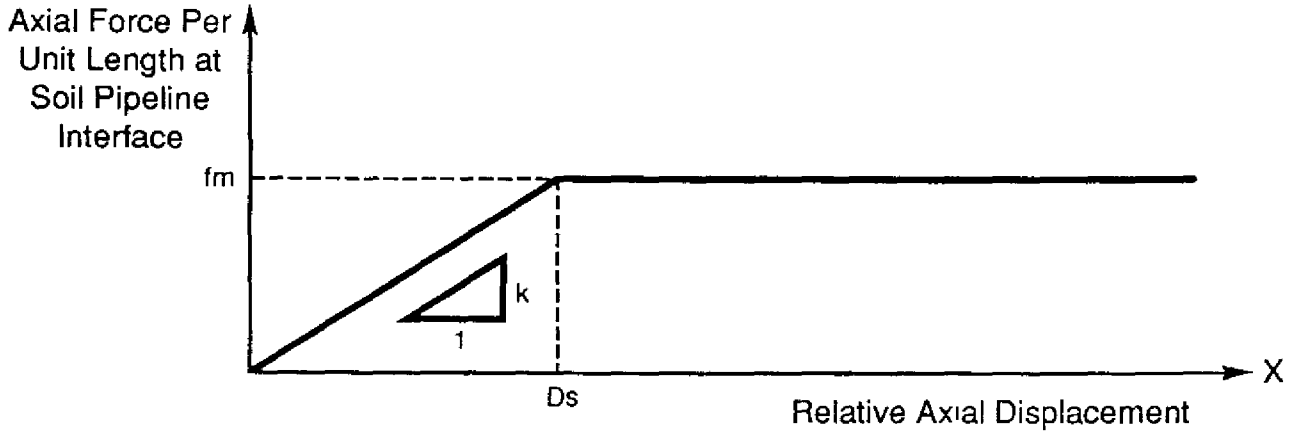

FIGURE 3-2 Assumed Axial Force vs. Relative Displacement Relation for Elastic Spring/Slider Model of the Soil-Pipeline Interface.

$$f_m = \mu \cdot \gamma H \cdot \frac{(1 + K_0)}{2} \cdot \pi\phi \tag{3.1}$$

where μ is the coefficient of friction at or near the soil/pipeline interface, γ is the unit weight of the soil, H is the depth to the pipe centerline, K_0 is the coefficient of lateral earth pressure and ϕ is the outside diameter of the pipe.

Experimental studies have shown that the coefficient of friction, μ, between the soil and the pipeline depends mainly on the nature of the pipe surface, the angularity of the soil grains and the relative roughness of the pipe surface with respect to the soil grains. Results obtained by Kulhawy and Peterson [14] show that for rough concrete pipe surfaces, slippage occurs in the soil near the interface and that $\mu \simeq \tan\theta$ where θ is the angle of shearing resistance of the soil. For the case of a concrete pipe with smooth surfaces, slippage occurs at the interface for $\mu/\tan\theta$ ranging from 0.8 to 1.0, with a mean value of 0.9 ($\mu \simeq 0.9 \tan\theta$). Colton et al. [13] noticed that for pipes wrapped with plastic covering, slippage happens in the soil near the pipe rather than at the interface. The reason is that the soil grains become partially embedded in the plastic cover at the interface. Brumund and Leonards [15] also observed that $\tan\theta$ is an upper bound for μ, regardless of the rate at which slippage is initiated. Two types of surfaces were studied: Mortar/Sand and Polished Steel/Sand. The result for the first surface was similar to Kulhawy and Peterson's result for concrete surfaces. For the Polished Steel surface, the mean value of μ is equal to 0.5 $\tan\theta$. Based on these experimental results, the coefficient of friction for normal (i.e. unpolished) steel pipe is taken to be that for concrete pipe with smooth surface, that is

$$\mu = 0.9 \tan\theta \tag{3.2}$$

The magnitude of K_0 for normally consolidated cohesionless soil has been reported to range from 0.35 to 0.47 (Perloff and Baron [16]). However, because of the backfilling and compaction of the soil around the pipeline, one expects K_0 to be somewhat larger. O'Rourke et al. [17] recommend $K_0 = 1.0$, as a conservative estimate for most conditions of pipeline burial.

3.2 Axial Stiffness

The technical literature contains a number of relations for the initial axial stiffness, k. For the plane strain case, Novak et al. [18] presented the initial axial stiffness as a function of frequency with values ranging from about 1.50 to 2.75 times the dynamic soil shear modulus, G ($1.50\ G \leq k \leq 2.75\ G$). O'Leary and Datta [19] calculated k at low frequency to be about two times G. In their comparison of the observed behavior of a tunnel with a multiple mass–spring model, Shibata et al. [20] have used $k = G$. In a Japanese design procedure for buried pipelines, Kuboto Ltd [21] suggests a value of $k = 3.0\ G$. Based upon an analytical study of piles, O'Rourke and Wang [22] use $k = 2.0\ G$. These analytical results suggest $1.0G \leq k \leq 3.0\ G$.

Colton et al. [13] performed full–scale experiments which studied axial soil–pipe interaction for buried pipeline. ElHmadi and O'Rourke [23] used the Colton results to back calculate the equivalent value for k They found that $1.57G \leq k \leq 1.70\ G$ when G is evaluated for the expected level of soil strain. Based upon the analytical and experimental values mentioned above, the initial spring stiffness k is taken herein as twice the soil shear modulus, or

$$k = 2.0\ G \tag{3.3}$$

The procedure used to evaluate G for the appropriate level of soil strain follows that in ElHmadi and O'Rourke [24].

3.3 Relative Axial Displacement for Slippage

As noted previously, the relative axial displacement for slippage at or near the soil–pipe interface, D_s, is simply f_m/k as shown in Figure 3–2. Table 3.1 lists D_s for various values of the pipe diameter, ϕ, and burial depth to the top of the pipe, $C = H - \phi/2$, evaluated for a soil unit weight of 100 pcf. Table 3.I(a) is for a coefficient of friction $\mu = 0.45$ which corresponds to an angle of shearing resistance of $\theta = 27°$. Tables 3.I(b) and 3.I(c) are for coefficients of friction of 0.60 and 0.75 respectively, which correspond to $\theta = 34°$ and $40°$.

As shown in Table 3–I the D_s values are increasing functions of μ, ϕ and C. However, for what is felt to be a reasonable range of parameters, all D_s values are less than 0.075 inches. Note in this regard that Holloway [25] infers values in the 0.01 to 0.04 in. range for the

relative displacement at slippage based upon tests of soil/pile interaction.

The small values for D_s suggests a simplified model for soil–pipe interaction. This simplified model, shown in Figure 3–3, assumes that the soil spring is rigid ($k = \infty$ and $D_s = 0$). That is, the spring portion of the spring slider is neglected.

In the next two sections, the response of buried pipelines subject to two idealized patterns of longitudinal PGD will be evaluated using both the elastic spring/slider model in Figure 3–2 and the rigid spring/slider model in Figure 3–3. In subsequent sections, the rigid spring/slider model is used to evaluate response for two additional PGD patterns.

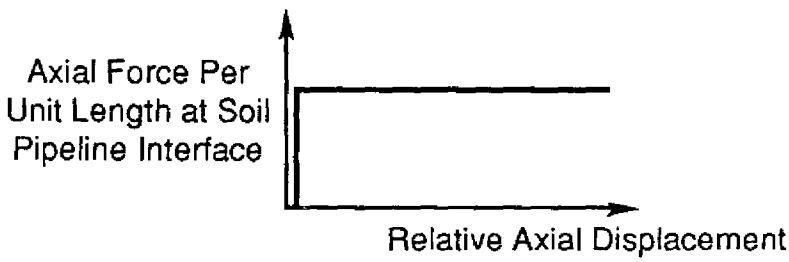

FIGURE 3-3 Assumed Axial Force vs. Relative Displacement Relation for Rigid Spring/Slider Model of the Soil-Pipeline Interface.

Pipe Diameter ϕ (in)	Burial Depth to Top of Pipe, C (ft)		
	3 (.91 m)	6 (1.83 m)	9 (2.74 m)
12 (30.5 cm)	.004	.007	.010
30 (76.2 cm)	.011	.018	.026
48 (122 cm)	.020	.032	.044

(a) Coefficient of Friction $\mu = 0.45$.

Pipe Diameter ϕ (in)	Burial Depth to Top of Pipe, C (ft)		
	3 (.91 m)	6 (1.83 m)	9 (2.74 m)
12 (30.5 cm)	.005	.009	.013
30 (76.2 cm)	.014	.024	.034
48 (122 cm)	.027	.043	.059

(b) Coefficient of Friction $\mu = 0.60$.

Pipe Diameter ϕ (in)	Burial Depth to Top of Pipe, C (ft)		
	3 (.91 m)	6 (1.83 m)	9 (2.74 m)
12 (30.5 cm)	.006	.011	.016
30 (76.2 cm)	.018	.030	.043
48 (122 cm)	.033	.054	.074

(c) Coefficient of Friction $\mu = 0.75$.

Table 3–I Relative Axial Displacement, D_s, in inches, for Slippage at the Soil/Pipe Interface evaluated for Unit Weight of Soil $\gamma = 100$ pcf (1610 kg/m^3).